

Development and Analysis of a Probabilistic Reasoning Methodology for Spectrum Situational Awareness and Parameter Estimation in Uncertain Environments

Todd Martin

Volgenau School of Engineering
George Mason University
Fairfax, Virginia USA
tmartin@gmu.edu

KC Chang

Volgenau School of Engineering
George Mason University
Fairfax, Virginia USA
kchang@gmu.edu

Abstract – Advancements and proliferation of wireless devices and capabilities have expanded the need for spectrum situational awareness in support of mobile applications. Accurate representations of spectrum usage parameters, however, are limited by the ability to attain sufficiently accurate information in environments characterized by significant uncertainty.

This paper describes the design and characterization of a probabilistic reasoning methodology for spectrum situational assessment. The approach uses Functional Causal Models—a form of Bayesian Networks—to represent the propagation environment and enables parameter estimation in uncertain environments. The general model is described and a simulation implementation is used as a basis for quantitative and qualitative characterization.

Results demonstrate the degree of uncertainty reduction for various parameters as functions of prior beliefs and consistency with theoretical predictions. Path loss estimation error was significantly reduced to within 10 dB of true conditions via Bayesian updating with several cases showing errors of less than 5 dB. Estimation errors of transmitted power were marginally reduced in the selected scenarios, and path distance could not be reliably estimated. Thus the proposed approach produces path loss estimates that could enable applications such as Dynamic Spectrum Access systems to operate with acceptable levels of risk.

Keywords: Probabilistic reasoning, situational awareness, estimation, Bayesian Networks, wireless communications.

1 Introduction

Spectrum situational awareness (SA) provides a characterization of what radio frequency (RF) emitters exist in a given area, their location, and other information such as usage patterns. As wireless device applications grow, spectrum SA has increased in applicability and importance. Spectrum SA was once primarily associated with electronic intelligence (ELINT) for military and intelligence organizations. The proliferation of wireless devices and

their associated computational capabilities have enabled subsets of ELINT capabilities to be developed in support of other applications. Search and rescue (SAR) organizations apply spectrum SA for geolocation of emergency beacons. Spectrum managers and commercial wireless service providers (e.g., broadband and cellular companies) seek to understand spectrum usage for wireless network deployment planning and identifying sources of interference [1,2]. More recently, commercial and government spectrum and wireless organizations (regulators and users) have been developing methods for dynamic spectrum access (DSA) [3,4], which depends upon accurate path loss estimates and other usage information for effective operation. Communications satellite payload management also relies heavily upon spectrum SA for understanding signal propagation characteristics and assessing interference [5].

In many of these applications, spectrum SA has significant sources of uncertainty that hinder or limit performance. RF emitter information (e.g., location and transmit power) is not readily known in many instances, and uncertainty regarding signal propagation characteristics also exists. These uncertainties can generate significant errors when estimating parameters such as path loss and emitter location [6].

Several estimation uncertainty reduction techniques have been studied and applied, but each encounters practical limitations. Distributed sensing is often proposed as a means to reduce uncertainty regarding channel and emitter characteristics from detected signals [7]. If the emitter-to-sensor channel characteristics are sufficiently uncorrelated (e.g., the sensors are geographically separated), detection and estimation accuracy can improve. Some systems, however, may have only a local sensor available or have limited capability to support data exchange among sensors or with a fusion center. Spectrum SA systems with limited cooperative sensing capabilities may use locally-stored databases that catalogue known emitter characteristics and estimates of local signal propagation characteristics [2,8]. Database-oriented approaches, however, are of limited use in highly-dynamic situations with significant mobility and propagation environment variations.

To address those limitations, a probabilistic reasoning approach for spectrum SA has been proposed [9]. The technique uses Bayesian Network (BN) models of the propagation environment and spectrum users as part of a spectrum SA and reasoning capability. Input parameter estimates may come from local sensing, distributed sensing, database sources, or a fused estimate from multiple modes. The model is thus applicable to distributed and stand-alone systems as well as fixed and mobile implementations. In theory, the SA accuracy adapts to the diversity and availability of information, information sources, and information quality. Consequently, decisions can then be made with insight into risks associated with SA uncertainty.

This paper presents the design and assessment of the propagation estimation portion of the model, which is foundational to the probabilistic spectrum SA model. While the methodology has been developed and applications discussed [9,10,11], a sufficient characterization of an implementation has not been available. The intent of the paper is to provide a quantitative and qualitative characterization using a computer-simulation. Specifically, the analysis addresses spectrum SA estimation performance for path loss, transmitted power, and path distance.

The next section provides an overview of the spectrum SA model and provides the design detail of the propagation estimation model assessed in this paper. An implementation is described in Section 3 along with an assessment of results and discussion of insights.

2 Probabilistic SA and Reasoning Model

The conceptual development of a spectrum SA model is described in the context of a DSA system [6,9,10] and applied in a satellite communications (SATCOM) [11] context in prior articles. The methodology uses a Functional Causal Model (FCM)—a type of BN that uses the system of equations describing the underlying phenomenology to specify the parameters and general structure BN structure [12].

The specific model evaluated in this study represents the effects of path loss (L_{path}) and transmitted signal power (P_{tx}) on the power received (P_{rx}) by a sensor. The functional representation used for each of these parameters is given (in dB scale) by the following equations:

$$L_{path} = 10\alpha \log_{10} \left(\frac{c}{4\pi f d} \right) \quad (1)$$

$$P_{sig,rx} = P_{tx} - L_{path} \quad (2)$$

$$P_{rx} = 10 \log_{10} (10^{0.1P_{sig,rx}} + 10^{0.1N}); \quad (3)$$

with parameters having the following definitions:

- c : speed of light (3×10^8 m/s)
- α : propagation decay exponent
- f : channel frequency
- d : distance between transmitter and receiver
- $P_{sig,rx}$: received power of the transmitted signal

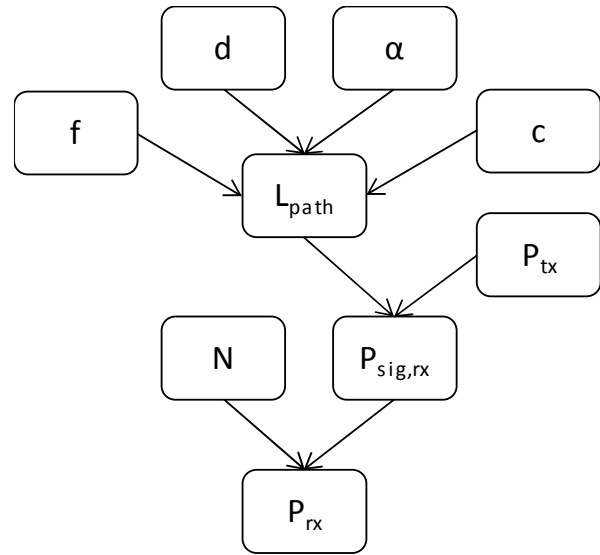


Figure 1: Spectrum SA Bayesian Network representation

- N : receiver system noise power
- P_{rx} : total received RF power (signal plus noise)

Those three equations form a system of functions that is represented by the FCM shown in Figure 1.

While the speed of light c and channel frequency f are known parameters and may generally be treated as constants, determinations of the other independent (non-child) parameters must be observed and characterized by in situ observations. Receiver noise N can be estimated by

$$N = 10 \log_{10}(kT_0B) + F \text{ (dB)}, \quad (4)$$

where:

- k : Boltzmann's Constant (1.38×10^{-23} J/K)
- T_0 : noise temperature
- B : noise-equivalent bandwidth
- F : receiver (system) noise figure [13].

Alternatively, N can be directly determined by directly observing the channel in the absence of noise. The remaining parameters—the propagation decay exponent α , path distance d , and transmitted power P_{tx} —generally cannot be directly measured or estimated through spectrum sensing observations, thus requiring information from some other source. Transmitted power information can be derived from various data sources such as existing and proposed regulatory databases [4,8], from which a system could determine the range of transmitter powers associated with devices using the spectrum being monitored. Similarly, the databases would provide the locations of fixed (non-mobile) transmitters in many spectrum bands allowing the path distance d to be determined (assuming the sensor can determine its own location). If the signal source is not known or is determined to be mobile, the path distance will be uncertain. Attaining a priori estimates for the path loss exponent can be more challenging, as the nature of signal attenuation can vary significantly in a given area [14]. Most likely, a priori attenuation characteristics for a given

location would be derived from propagation studies and terrain-based models such as the Irregular Terrain Model [15]. Alternatively, propagation characteristics could be estimated from signals received from emitters having known characteristics (e.g., frequency and antenna height) that are similar to those of the emitter of interest.

With the spectrum SA model, each of the parameters having some uncertainty is modeled as a random variable. The expected receive power therefore has a probability distribution given by:

$$p(P_{rx}|\alpha, d, P_{tx}, N) = p(P_{rx}|P_{sig,rx}, N) \cdot p(P_{sig,rx}|L_{path}, P_{tx}) \cdot p(L_{path}|\alpha, d)p(P_{tx}) \cdot p(\alpha)p(d)p(N). \quad (4)$$

As previously discussed, parameters commonly of interest for spectrum SA estimation applications are the transmitter power P_{tx} , path loss L_{path} , and transmitter location (as determined by path distance d). Updates for these parameters can be found by sensing the received power P_{rx} and performing Bayesian updating.

The next section presents an implementation of the spectrum SA model and provides some analyses of its characteristics and performance under a range of conditions.

3 Simulation Results and Analyses

The spectrum SA model from Figure 1 was implemented using the Netica Java API¹ as shown in Figure 2 with custom Java code for managing network settings and commands. Analyses were conducted to assess the model's ability estimate parameters such as path loss, transmitter power, and the propagation decay exponent given initial levels of uncertainty and observations of a received signal.

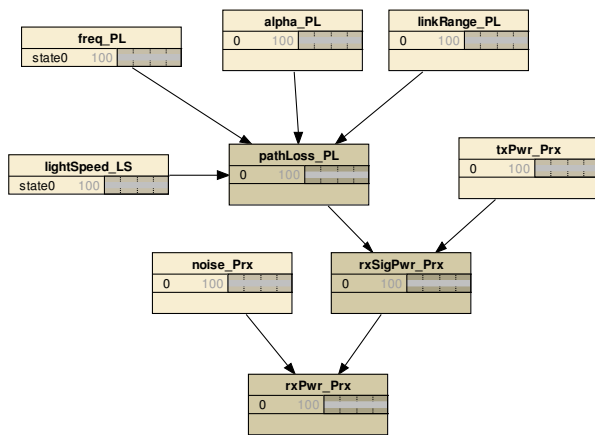


Figure 2: Netica implementation of the spectrum SA model used in the analysis.

The analyses are grouped into three categories based on prior uncertainties of the model parameters. The first

analysis, which is presented in the following section, investigates model behavior and parameter estimation capabilities when prior uncertainty exists for the propagation decay exponent α , the transmitted power P_{tx} , and the distance d between the transmitter and sensor. Section 3.2 presents analysis when d is known, and Section 3.3 presents analysis when P_{tx} is known.

3.1 Unknown P_{tx} , α , and d

The initial prior values used in the analyses presented in this section are shown in Table 1. The frequency f being monitored is a known value based on the settings of the sensor. The receiver noise N is a measureable parameter and takes a single value for the purposes of this assessment. The propagation exponent α is set as a normal distribution that ranges from a lower limit of 2 (free space propagation) to 6 (significant propagation loss due to foliage, buildings, etc.). The transmit power P_{tx} is represented by a uniform distribution ranging from 24 dBm (~300 mW) to 36 dBm (4 W), indicating significant uncertainty across a wide range of possible transmitter types. Finally, the distance d is similarly a uniform distribution, with a maximum of $d=10$ km.

Table 1: Spectrum SA model parameter prior belief settings

Parameter	Prior
Frequency (f)	1 GHz
Distance (d)	U(1,10000) m
Propagation exponent (α)	N(4,1), $2 < \alpha < 6$
Transmit Power (P_{tx})	U(24,36) dBm
Receiver Noise (N)	-110 dBm

The prior values from Table 1 produce the prior path loss L_{path} and received power P_{rx} probability distributions shown in Figure 3. The path loss prior distribution is found to have significant uncertainty with a mean of -201 dB and variance of 53.6. The range of values is driven by the combinations of $\{\max(\alpha), \min(P_{tx}), \max(d)\}$ for the maximum (i.e., most negative) path loss and $\{\min(\alpha), \max(P_{tx}), \min(d)\}$ for the minimum path loss. The received power distribution appears to show significantly less uncertainty with a mean of -106 dBm and variance of 11.6. The distribution, however, has a lower bound at -111 dBm but a long tail extending to -1.5 dBm for a total span of nearly 100 dBm.

With these priors in place, the simulation model uses scenario parameters to determine the true received power measured at the receiver and reported to the spectrum SA model. The relevant scenarios are created from the set of parameter settings shown in Table 2. The values cover the uncertainty ranges of the corresponding spectrum SA uncertainty parameters from Table 1. A signal power variance of 1 dB is also added to the scenario, which simulates modest average power variations along the path from emitter to receiver (see Figure 4, top).

¹ See www.norsys.com/netica-j.html

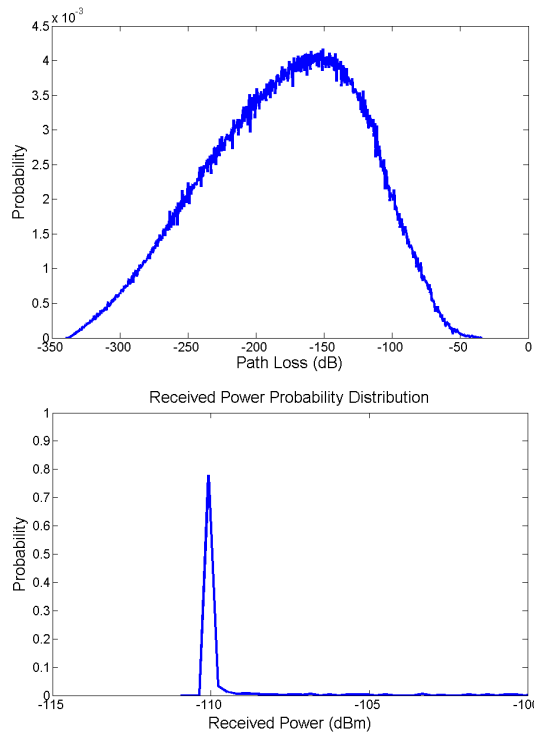


Figure 3: Path loss L_{path} (top) and received power P_{rx} (bottom) prior distributions.

Table 2: Simulation model scenario parameter settings

Parameter	Values
Transmit Power (P_{tx})	{24,30,36} dBm
Distance (d)	{1,...,10000} m
Propagation exponent (α)	{2,...,6}
Signal power variance	1 dB

With each scenario, the receiver uses a minimum detectable signal to noise ratio (SNR) threshold as a first step in the detection process. If the received signal is above the threshold SNR, the signal is declared detectable and sent to the spectrum SA model for estimating the unknown parameters. If the signal is below the threshold SNR, no detection is declared and the scenario generator advances to the next set of scenario parameter values. A SNR detection threshold of 0 dB is used for the scenarios presented here, allowing for a characterization of the model at low received signal levels.

When a set of scenario parameter values generates a detectable signal, the spectrum SA model treats it as an observed finding for the received power P_{rx} node. The remaining BN model parameters are updated based on the observation to produce posterior estimates.

Figure 4 provides an illustration of the observed signal power (P_{rx}) and updated (i.e., posterior) path loss L_{path} distribution following a single observation for one of the scenarios. The mean received power is found to be -42.5 dBm from a signal transmitted at 24 dBm, corresponding to

a -66.5 dB mean path loss. The prior and updated estimates for L_{path} in the bottom graph of Figure 4 demonstrate the significant change given only a single observation. While the prior had a mean of -201 dB and variance of 53.6, the updated L_{path} estimate is -73.2 dB with a variance of 4.1. The remaining spectrum SA uncertainty parameters are similarly updated and reported in Table 3.

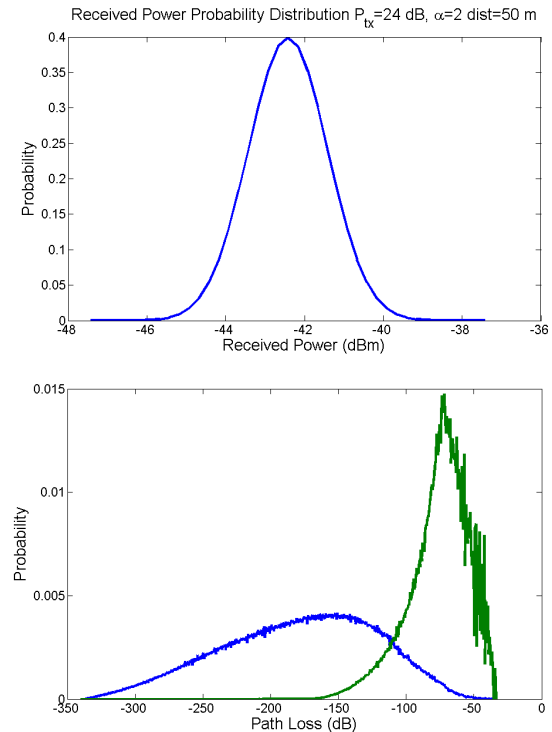


Figure 4: Received power P_{rx} distribution (top) and resulting path loss L_{path} prior and posterior beliefs (bottom) after a single P_{rx} observation.

Table 3: Posterior probability distributions of the SA model uncertainty parameters after the first observation for the case from Figure 1.

Parameter	Posterior Distribution
L_{path}	$\mu = -73.2, \sigma^2 = 4.1$ dB
$P_{sig,rx}$	$\mu = -42.4, \sigma^2 = 0.96$ dBm
d	$\mu = 16.9, \sigma^2 = 23.4$ m
α	$\mu = 2.9, \sigma^2 = 0.57$
P_{tx}	$\mu = 30.9, \sigma^2 = 3.8$ dBm

The updated beliefs can now be used as prior estimates for the subsequent observation. Keeping the scenario parameters constant, the model makes additional observations, each followed by belief updating. Continuing with the example, Figure 5 shows the estimation results for the L_{path} estimate as a function of observation-update cycles. The graph includes the mean estimate as well as the 95% and 99% quantiles.

The data show a significant reduction in estimation error and uncertainty. While only one case is shown here, the other combinations of scenario parameters produce

comparable results. The mean L_{path} estimate converges to within 8 dB of the true path loss—and in some cases to within 3 dB—representing an improvement of almost 200 dB from the prior estimate mean. The convergence occurs quickly, generally within five (5) observations. The uncertainty is also greatly reduced within the first five (5) observations. Continued observations, however, produce over-confident results with the true path loss falling outside of the 99% quantile by the 7th observation.

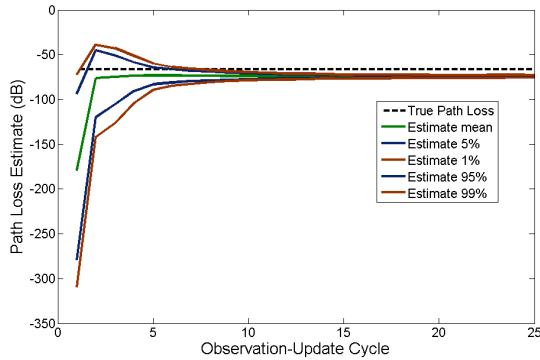


Figure 5: Example path loss L_{path} estimation error as a function of Bayesian update cycles.

Data analysis demonstrates that the magnitude of path loss estimation error depends on the difference between the true transmit power and mean of the transmit power prior distribution used in the model. Figure 6 shows the path loss estimation error as a function of received power P_{rx} delineated by the true transmitted power $P_{tx,true}$. It is easily seen that the path loss estimation error is affected by the transmitted power.

Further analysis demonstrates that the effect is created specifically by the difference between the estimate and true P_{tx} as derived in [6]. Estimation error data for P_{tx} shown in Figure 7 demonstrates that the relationship between L_{path} and P_{tx} is consistent with (13a) in [6], which is given by

$$\Delta\mu_{L_p} = \mu_{P_{tx,true}} - \mu_{P_{tx,est}}, \quad (5a)$$

$$\Delta\mu_{L_p} = -\Delta\mu_{P_{tx}}, \quad (5b)$$

where $\Delta\mu_{L_p}$ is the mean path loss error and $\Delta\mu_{P_{tx}}$ is the mean transmitted power estimate error. Comparing data from Figure 6 and Figure 7, it can be shown that the errors are of the same magnitude but opposite signs. The consequence is that path loss estimation is limited by the extent to which transmitted power can be estimated and vice versa.

With the propagation model used in this study, path loss estimates are a function of the propagation loss exponent and distance. The estimation error relationship for these three parameters are defined in [6] by (15) by

$$\Delta\mu_{L_p} = \mu_{\alpha_{true}}\mu_{f_{d,true}} - \mu_{\alpha_{est}}\mu_{f_{d,est}} \quad (6)$$

where μ_{fd} is given by

$$\Delta\mu_{fd} = E \left[10 \log_{10} \left(\frac{c}{4\pi fd} \right) \right]. \quad (7)$$

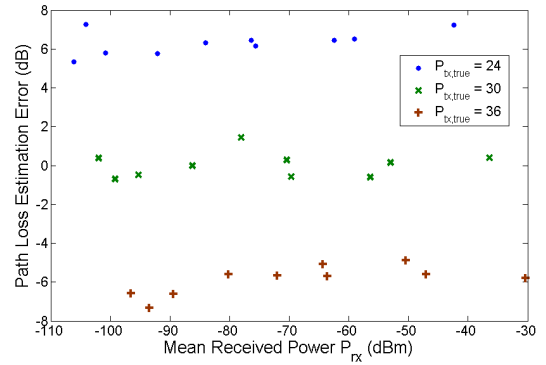


Figure 6: Path loss L_{path} estimation error as a function of mean received power P_{rx} for each true transmitted power P_{tx} .

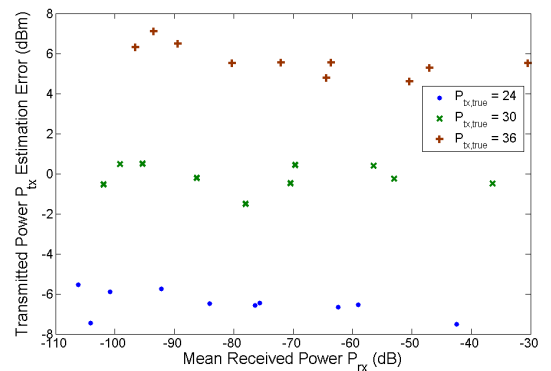


Figure 7: Transmitted power P_{tx} estimation error as a function of mean received power P_{rx} for each true transmitted power P_{tx} .

The simulation results shown are found to be consistent with those theoretical representations. The path loss exponent α and link distance d estimates behave similar to that shown for path loss L_p , producing an over-confident estimate after several observation-update cycles. The magnitude of the estimation errors, however, is much greater for the link distance estimate d as shown in Figure 8. The increased relative error is due to the logarithmic relationship between d and the other parameters as shown in (1) and (7). Variations in link distance have a much smaller effect on path loss relative to variations in the path loss exponent. Small errors in path loss L_{path} estimation can therefore result in large errors in link distance d estimation.

Data analyses show two further characteristics of link distance estimation. First, link distance was consistently estimated to be less than 50 m (the region where distance variations have a greater effect on path loss) regardless of the true link distance. The data in Figure 8 (upper graph) consequently shows that the magnitude of link distance estimation errors increase with true link distance. Second, Figure 8 (lower graph) shows no notable influence of path loss exponent on distance estimation capabilities.

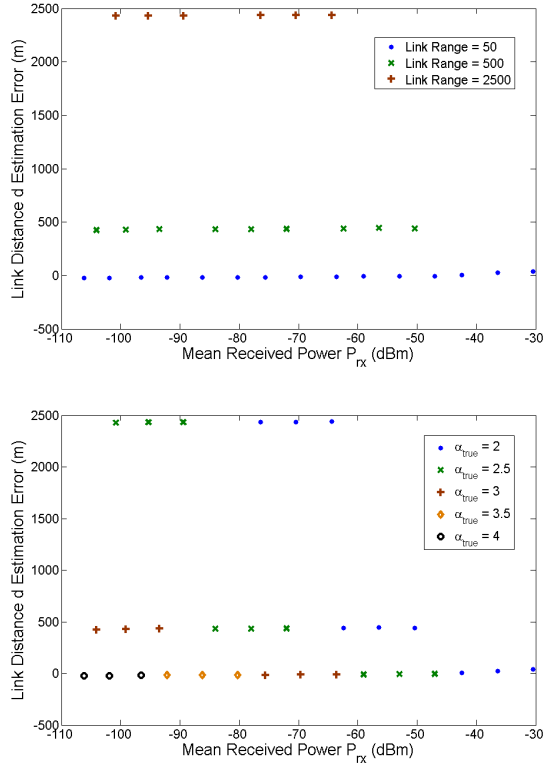


Figure 8: Link distance d estimation error as a function mean received power for various true link distances and path loss exponents.

The path loss exponent α error estimation data, however, shows dependencies on the true α and d values. Similar to link distance estimates, Figure 9 (upper graph) shows a clear trend of increased estimation error with the true path distance. Additionally, Figure 9 (lower graph) shows a dependency on the true path loss exponent. This trend is predicted by (6) and (7), in which an increase in link distance error must be offset with an increase in path loss exponent error for a given path loss estimation error $\Delta\mu_{Lp}$.

3.2 Estimating L_{path} , P_{tx} , and α with known d

For this set of scenarios, the location of the transmitter is known while the remaining uncertainty parameters are estimated as described in the previous analysis. The link distance is set at $d=\{50, 500, 2500\}$ meters while the remaining parameters are defined as before (see Table 1).

Path loss L_{path} estimation error exhibits similar behavior as shown in the previous set of scenarios as shown in Figure 10. The errors, however, are shifted to the positive by about 1.5 dB (see also Figure 13). This gives an error range between -5 to 9 dB for this case compared with an error range of ± 8 dB in the first case (see Figure 6). Transmitted power P_{tx} estimation errors are correspondingly shifted consistent with (5) as shown in Figure 11.

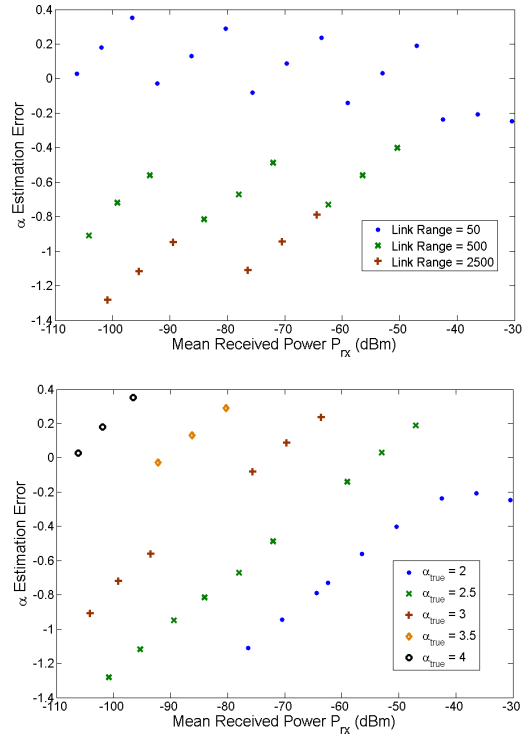


Figure 9: Propagation loss exponent α error as a function of mean received power for various link ranges (top) and propagation exponents (bottom).

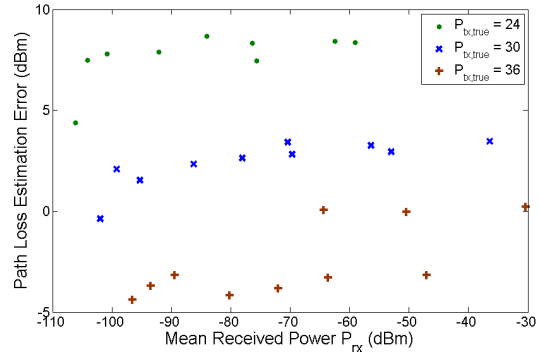


Figure 10: Path loss L_{path} estimation errors for known link distance d as a function of mean received power.

Path loss exponent α estimation errors are shown in Figure 12 to be greatly reduced compared to the prior case as predicted by (6). For this case, $\mu_{f_{d,true}} = \mu_{f_{d,est}}$, giving

$$\Delta\mu_{Lp} = (\mu_{\alpha_{true}} - \mu_{\alpha_{est}})\mu_{f_d} = \Delta\mu_{\alpha}\mu_{f_d}. \quad (8)$$

Since the estimation error is now independent of distance errors and $|\mu_{f_d}| > 1$, the path loss exponent error will always be less than the path loss error, i.e., $\Delta\mu_{\alpha} < \Delta\mu_{Lp}$. Note also that Figure 12 shows that $\Delta\mu_{\alpha}$ is influenced by transmitted power P_{tx} , as can be seen by substituting (5b) into (8). In the prior case, this influence was mitigated by link distance errors.

These results show that knowing the link distance may bias path loss L_{path} and transmitter power P_{tx} estimation errors, but will always reduce the path loss exponent α estimation error.

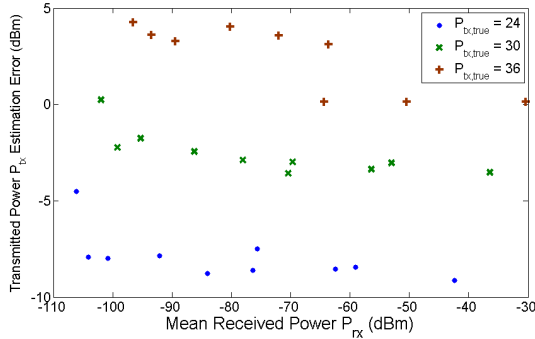


Figure 11: Transmitted power P_{tx} estimation errors for known link distance d as a function of mean received power.

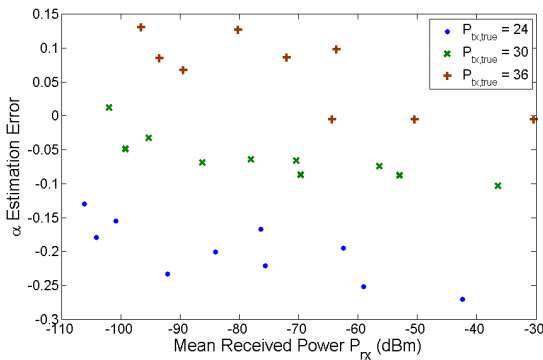


Figure 12: Path loss exponent α estimation errors for known link distance d as a function of mean received power.

3.3 Estimating L_{path} , α , and d with known P_{tx}

For this set of scenarios, the transmitted power P_{tx} is known while the remaining uncertainty parameters are estimated as described in the previous analyses. Transmitted power levels are set at $P_{tx} = [24,30,36]$ dBm while the remaining parameters are defined as in Table 1.

As expected, L_{path} estimation error becomes negligible (less than 1 dB) as shown in Figure 14. Knowing both P_{tx} and P_{rx} (along with system noise N) provides an exact solution to L_{path} as defined in (2) and (3). The distribution of the L_{path} estimate, however, is overconfident as previously described.

The estimation error for d shows the same behavior as found in the first set of scenarios. Range is consistently estimated at $d < 100$ m regardless of true distance, P_{tx} , or α . Estimation error for α , however, is shown in Figure 14 to have more variation with true α than the prior cases.

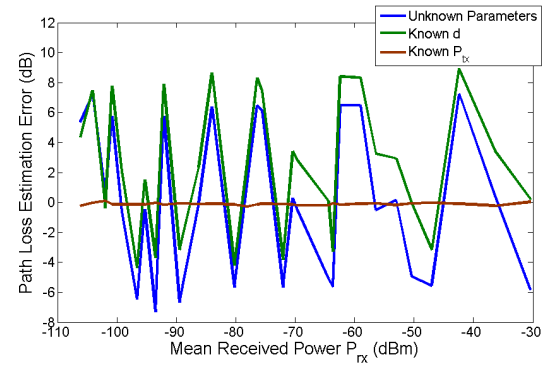


Figure 13: Path loss L_{path} estimation error for the three scenarios.

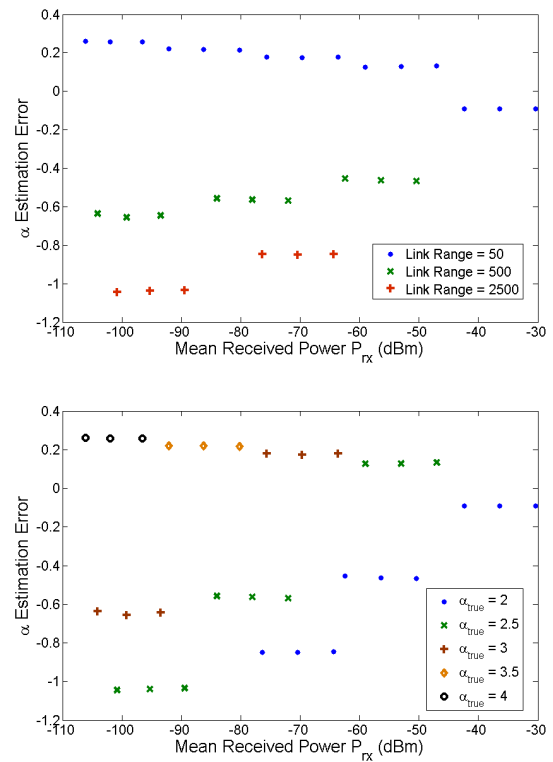


Figure 14: Path loss exponent α estimation error as a function of mean received power for various true link ranges (top) and propagation exponents (bottom).

3.4 Summary and Concluding Remarks

Parameter estimation capabilities are found to vary greatly by parameter for the model analyzed here. Path loss estimates were greatly improved after several observation-update cycles, as were path loss exponent estimates. Transmitted power estimates were marginally improved, and link distance estimates were shown to be very poor due to its logarithmic relationship to the other parameters. One issue to be addressed in future work is the over-confidence produced after several observation-update cycles.

Interactions among parameter estimates and associated errors were found to be consistent with theoretical formulations developed in [6]. Furthermore, knowing various parameter values produced mixed results with respect to estimation of the remaining parameters.

The results indicate that the probabilistic spectrum SA model may be more beneficial for some applications over others. Uses involving path loss estimation but having significant environmental uncertainty—such as DSA—may benefit from the significant reduction in path loss uncertainty. Other applications such as geolocation system relying on distance estimates, however, would not be able to use the model studied here due to the inability to attain useful distance estimates.

Future efforts will further explore the characteristics of the model and evaluate its utility in various system models. Analysis will be conducted using a range of probability distribution types and values to understand their effect on estimation accuracy. The performance predicted by the simulations will also be experimentally validated using spectrum measurement data. Finally, investigations will evaluate means for generating prior estimates from available information sources including regulatory information, equipment standards, and multi-modal sensing.

References

- [1] E. O. Nuallain and C. Anderson, “Real-Time Radio Environment Mapping for Cognitive Radio,” in *Wireless Research Collaboration Symposium (NWRCS)*, 2014 National, 2014, pp. 64–68.
- [2] W. Heisey, W. Kline, H. Zebrowitz, R. Poe, S. Sharma, A. Cortese, M. Hoque, F. Loso, and Y. Levy, “Automated Spectrum Plan Advisor for On-The-Move Networks,” in *IEEE Military Communications Conference, 2006*. October 23-25, 2006.
- [3] “The Dynamic Spectrum Alliance: A New Global Initiative to Help Governments Address Wireless Data Growth and Close the Digital Divide” *Business Wire*,” 18-Jun-2013.
- [4] “Report to the President: Realizing the Full Potential of Government-Held Spectrum to Spur Economic Growth,” President’s Council of advisors on Science and Technology, Executive Office of the President, Washington DC, July 2012.
- [5] D. Whitefield and R. Gopal, “Capacity enhancement with dynamic resource management for next generation satellite systems,” in *IEEE Military Communications Conference, 2005. MILCOM 2005*, 2005, pp. 761–767 Vol. 2.
- [6] T. Martin and K.C. Chang, “Situational Awareness Uncertainty Impacts on Dynamic Spectrum Access Performance,” in *17th International Conference on Information Fusion (FUSION2014)*, Salamanca, Spain, 2014.
- [7] R. Umar and A.U.H. Sheikh, “A comparative study of spectrum awareness techniques for cognitive radio oriented wireless networks,” *Physical Communication*, vol. 9, pp. 148–170, Dec. 2013.
- [8] Federal Communications Commission, Spectrum Dashboard, <http://reboot.fcc.gov/reform/systems/spectrum-dashboard>.
- [9] T. Martin and K.C. Chang, “A causal reasoning approach to DSA situational awareness and decision-making,” in *16th International Conference on Information Fusion (FUSION2013)*, Istanbul, Turkey, 2013, pp. 638–646
- [10] T. W. Martin and K.C. Chang, “A Quantitative Analysis on the Impact of Spectrum Access Policy Flexibility and DSA System Capability on Spectrum Sharing Potential,” Social Science Research Network, Rochester, NY, SSRN Scholarly Paper ID 2242177, <http://ssrn.com/abstract=2242177>, Mar. 2013.
- [11] T. Martin, K.C. Chang, Xin Tian, Genshe Chen, Tien Nguyen, K.D. Pham, and Erik Blasch, “A Probabilistic Situational Awareness and Reasoning Methodology for Satellite Communications Resource Management,” *Aerospace Conference, 2015 IEEE*, March 2015.
- [12] J. Pearl, *Causality: Models, Reasoning, and Inference*, 2nd ed. Cambridge ; New York: Cambridge University Press, 2009.
- [13] J. S. Seybold, *Introduction to RF Propagation*. Hoboken, N.J: Wiley, 2005.
- [14] J. R. Hampton, N. M. Merheb, W. L. Lain, D. E. Paunil, R. M. Shuford, and W. Kasch, “Urban propagation measurements for ground based communication in the military UHF band,” *IEEE Transactions on Antennas and Propagation*, vol. 54, no. 2, pp. 644–654, Feb. 2006.
- [15] G.A. Hufford, A.G Longley, and W.A Kissick, “A Guide to the Use of the ITS Irregular Terrain Model in the Area Prediction Mode,” US Department of Commerce, Technical Report 82-100, April 1982.